

# Extracting the pectoral muscle in screening mammograms using a graph pyramid

Fei Ma Mariusz Bajger Murk J. Bottema  
School of Informatics and Engineering, Flinders University  
PO Box 2100, Adelaide SA, 5001  
email: ma0029@infoeng.flinders.edu.au

## Abstract

*A graph based method is introduced to segment the pectoral muscles in screening mammograms. An adaptive pyramid is used to segment the mammogram into a number of components. Components forming the pectoral muscle are identified based on position, intensity, and shape. The boundary of the union of these components forms an initial boundary that is refined via an adaptive deformable contour model. The method is tested on 83 medio-lateral oblique mammograms from the Mini-MIAS database. Segmentation results are evaluated in terms of the proportion of correctly assigned pixels. Performance compares well with existing methods based on Hough transform and on Gabor wavelets.*

## 1 Introduction

Breast cancer screening programs based on mammography are used in many countries to facilitate early detection of breast cancer. Normally mammograms are evaluated visually by radiologists for signs of cancer. Since the mid 1980's, many computer algorithms have been proposed for automating various aspects of detecting the presence of cancer in mammograms and commercial products now exist that implement some of these programs. While detection rates for automatic systems are quite high, the false positive detection rates are also high. Accordingly, work continues on improving all aspects of computer-aided detection (CAD) for mammography.

Accurate segmentation of the pectoral muscle is among the many tasks that is needed to improve CAD for mammography. The pectoral muscle is one of the few anatomical features that appears clearly and reliably in medio-lateral oblique (MLO) view mammograms. The pectoral muscle is an important landmark both for providing contextual information regarding anatomies and for image registration.

To a first approximation, the pectoral muscle appears as a bright triangular patch in the upper left or upper right corner (depending on right or left breast) of the image. This motivated initial algorithms based on the Hough transform [2] [4]. The pectoral muscle is usually not exactly triangular and more accurate segmentation was achieved by using Gabor wavelets to segment the pectoral muscle without assuming straight boundaries [5]. Aside from incorporating general shape and location assumptions of pectoral muscle, these methods rely only on local image information.

In this paper, graph theory methods are used in an effort to incorporate global image information in segmentation. Graph pyramids were introduced by Tanimoto and Pavlidis in 1975 [6] and have been applied widely in image processing. A graph pyramid is a stack of successively reduced graphs. At each level in the stack, the graph is a reduction of the graph at the previous level. A vertex of a graph at one level is connected to a number of vertices at the previous level. The vertex in the higher level is called the parent of the vertices in the previous level and the set of vertices to which the parent is connected in the previous level (the children) is called the receptive field of the vertex. The collection of graphs forms a multi-resolution description of the image, but unlike multi-resolution representations via wavelets or filter banks, the connectivity between layers provides a vehicle for tracking information from disparate regions of the image. The connectivity between layers may be based directly on image intensities or derived image properties, thus providing a flexible tool for associating information content.

This paper is arranged as follows. In section 2, adaptive pyramids (AP) are described in detail. In section 3, a method for extracting the pectoral muscle, including an adaptive deformable contour model to refine the pectoral muscle boundary, is presented and in section 4 the performance of the method on a standard set of mammograms is reported.

## 2 Adaptive pyramid

Many methods have been proposed in constructing a graph pyramid from an original image. A. Montanvert, P. Meer and A. Rosenfeld introduced a general framework for building a pyramid graph [3]. In this framework, the  $l + 1$  level graph  $G_{l+1} = (V_{l+1}, E_{l+1})$  is derived from the  $l$  level graph  $G_l = (V_l, E_l)$  by the following steps:

1. The selection of vertices  $V_{l+1}$  from  $V_l$ . The selected vertices from  $V_l$  are named the surviving vertices while the unselected vertices are named non-surviving vertices.
2. The connection of each non-surviving vertices to the surviving vertices. This step defines a receptive field and parent relationships between the corresponding two levels of graph pyramid.
3. A definition of the adjacency relationships between elements in  $V_{l+1}$  in order to define  $E_{l+1}$ .

Many algorithms following these steps have been proposed. One of these is the adaptive pyramid introduced by Jolion [1]. In this adaptive pyramid, a support set is first defined for each pixel. The support set  $S_{ij}$  of pixel  $(i, j)$  is the set of all the neighbors of  $(i, j)$ .  $S_{ij}$  is initialised as the  $3 \times 3$  neighborhood centered on  $(i, j)$ . Based on these support sets, an interest operator is introduced to determine survivor selection (step 1). This interest operator is not fixed. Any image characteristics, global or local, can be incorporated into the interest operator. For example, Jolion used the variance of the intensity values within receptive fields as the interest operator [1].

Three variables are involved in selecting surviving vertices; two binary state variables  $p_{ij}$ ,  $q_{ij}$ , and the outcome of the interest operator,  $v_{ij}$ . The selection process works in two steps. In the first step, the state variable  $p_{ij}$  is set as

$$p_{ij} = \begin{cases} 1 & \text{if } v_{ij} = \min\{v_{mn} : (m, n) \in S_{ij}\} \\ 0 & \text{otherwise.} \end{cases}$$

In the second step, the state variable  $q_{ij}$  is set and some of the  $p_{ij}$  is updated by

$$q_{ij} = \begin{cases} 1 & \text{if } p_{mn} = 0 \forall (m, n) \in S_{ij} \\ 0 & \text{otherwise.} \end{cases}$$

$$p_{ij} = 1 \quad \text{if } v_{ij} = \min\{v_{mn} : (m, n) \in S_{ij}, q_{mn} = 1\}.$$

A pixel  $(i, j)$  is retained for the next level if  $p_{ij} = 1$ .

To make the connection between the non-surviving pixels and the surviving pixels (step 2), a contrast operator is used. A non-surviving pixel  $(i, j)$  will be connected to its surviving neighbor  $(m, n)$ , if and only if

$$|\mu_{ij} - \mu_{mn}| = \min_{(k,l) \in S_{ij}} \{|\mu_{ij} - \mu_{kl}| : p_{kl} = 1\},$$

where  $\mu_{ij}$ ,  $\mu_{mn}$  and  $\mu_{kl}$  are the mean intensities of the receptive fields of  $v_{ij}$ ,  $v_{mn}$  and  $v_{mn}$ .

Whenever a non-surviving pixel  $(i, j)$  is connected to a surviving pixel  $(m, n)$ ,  $S_{mn}$  is updated by  $S_{mn} = S_{mn} \cup S_{ij}$ . Thus the new adjacency relationships are formed.

In the adaptive pyramid, a root extraction process is also introduced to detect the components of the original image during the construction of the pyramid. A non-surviving pixel  $(i, j)$  is called a root if and only if

$$|\mu_{ij} - \mu_{mn}| > R(\text{size}(i, j)),$$

where function  $R$  is defined by

$$R(x) = \begin{cases} \text{min\_contrast} & \text{if } x > \text{min\_size} \\ \text{min\_contrast} * e^{\alpha(\text{min\_size} - x)} & \text{otherwise} \end{cases}$$

The value of  $\alpha$  was chosen so that  $R(1) = 64$  as was done by Jolion [1]. The two parameters `min_contrast` and `min_size` will be discussed in section 3.1.

If a non-surviving pixel  $v_{ij}$  is identified as a root, it will be retained to be a survivor and will appear in the highest level graph. The root extraction process prevents some components of the original image from disappearing during the construction of the graph pyramid and promises that each component of the original image has a representative pixel in the highest level graph.

The highest level graph is reached when no survivor can be selected. All the remaining pixels are roots. Each pixel in this level graph represents a component of the original image. From the receptive fields of these representative pixels, we can trace all the pixels within the corresponding components.

## 3 Pectoral Muscle Extraction

### 3.1 Implementing Adaptive Pyramid

The adaptive pyramid segments the mammograms into many components. The two parameters, `min_contrast` and `min_size`, involved in the root extraction process, affect the number of the resulted components. A larger `min_contrast` allows more pixels to be merged together and thus produces fewer components. Conversely, a smaller `min_contrast` prevents pixels from merging together and thus produces more components. For segmenting the pectoral muscle, values `min_contrast = 5` and `min_size = 100` were used. These values were determined empirically.

With these values for `min_contrast` and `min_size`, the non-breast region typically appears as 1 to 3 components and the breast region, being more complex, appears as many small components (Figure 1).

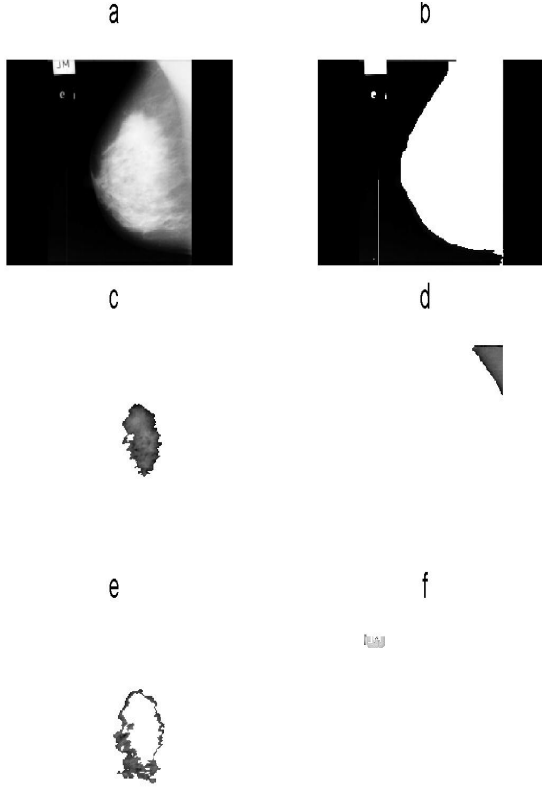


**Figure 1. Some components of image mdb00 after the segmentation. (a) is the original image, (b) is the non-breast component. (d) is a component of the pectoral muscle, (f) is an artifact, (c) and (e) are two components of the breast**

### 3.2 Adaptive Deformable Contour Model

After segmentation, the next task is to register the components belonging to the pectoral muscle. To register these components means to find their corresponding representative pixels in the highest graph. Three steps are used to do this job. First the component containing the upper left pixel (or right depending on left or right breast) is selected as a seed for the pectoral muscle. In the second step, components with intensities similar to the seed component and satisfying a set of size and position criteria are included as part of the pectoral muscle. These criteria are (1) the intensity of the component is within 80 units (on a scale of 0 - 255) of the intensity of the seed component, (2) the root of the component lies above the diagonal line of the region of interest (ROI) (the ROI is the smallest rectangle that includes the entire breast), (3) the distance between the root of the

component and the root of the seed component is less than half the length of the diagonal of the ROI. In the third step, shape information is used to further edit the collection of components assigned to the pectoral muscle. Components are excluded if (1) the geometric centre of the component is more than 30 pixels from the boundary of the seed component, (2) the ratio of the dimensions of the smallest box containing the component is less than 5, (3) the slope of either the left or right boundary of the component is negative for left breasts or positive for right breasts.

Experimental results show that these three steps identify most of the pectoral muscle components correctly. However, it is difficult to find exactly all the pectoral muscle components. Thus the boundary extracted from the identified components is often not precise. An adaptive deformable contour model was developed to refine the extracted pectoral muscle boundary.

Let  $V = v_1, v_2, \dots, v_N$  be the current pectoral muscle boundary with the ordered points  $v_i = (x_i, y_i), i = 1, 2, \dots, N$ . The adaptive deformable contour model works by moving the boundary through the spatial domain of the image to minimise a measure of energy based on the following formulas.

$$E_i = \alpha E_{in,i} + \beta E_{ex,i},$$

where  $\alpha, \beta$  are two weights controlling the internal and external energies  $E_{in,i}$  and  $E_{ex,i}$ . The internal and external energies are given by

$$\begin{aligned} E_{in,i} &= a_1 V'(v_i) + a_2 V''(v_i) \\ E_{ex,i} &= -|I_x(v_i)| / \max_I(I_x), \end{aligned}$$

where  $V'(v_i)$  and  $V''(v_i)$  are the first and second derivatives of the contour  $V$  at  $v_i$ ,  $I$  is the image, and

$$I_x = \frac{\partial I}{\partial x}.$$

The weights  $a_1$  and  $a_2$  are used to control the relative contributions of  $V'(v_i)$  and  $V''(v_i)$  and were fixed for this study at  $a_1 = 1$  and  $a_2 = 2$ .

The internal energy serves to reduce the curvature of the contour. This is important since the pectoral muscle has a general smooth straight shape. The external energy drives the contour toward strong edges in the image. This is important since the pectoral muscle is generally appears much brighter in the image than other tissue.

At every point  $v_i$ , the energies are computed on an asymmetric neighbourhood,  $\Omega_i$ , of size  $1 \times 9$  (Figure 2). More precisely,

$$\begin{aligned} \Omega_i &= [(x_i - 3, y_i), \dots, (x_i + 5, y_i)] \text{ (right breast)} \\ \Omega_i &= [(x_i - 5, y_i), \dots, (x_i + 3, y_i)] \text{ (left breast)}. \end{aligned}$$



**Figure 2. An example of the domain  $\Omega$  of  $v_i$ , In this case, the chest wall is left hand side positioned. The  $v_i$  is modified to  $e_j$  if the  $\min E_i$  is reached in  $e_j$ .**

Asymmetric neighbourhoods are used since the initial pectoral muscle boundary usually appears closer to the chest wall than the true boundary.

Unlike other deformable contour models, the weights for internal and external energy,  $\alpha$  and  $\beta$ , are adjusted automatically as follows.

$$\begin{aligned}\alpha &= |x_i - x_{i-1}| + |x_{i+1} - x_i| - 2 * d \\ \beta &= \exp((\max_{\Omega_i} |I_x| - \min_{\Omega_i} |I_x|) / \text{mean}_{\Omega_i} |I_x|) \\ d &= (x_1 - x_N) / N.\end{aligned}$$

When the point  $v_i$  is not close to the true pectoral muscle boundary,  $\beta$  will become big, and thus  $E_{ex,i}$  will take more weight in  $E_i$ . When the boundary is not smooth enough,  $\alpha$  will raise, and thus  $E_{in,i}$  will take more weight.

The elements of  $\Omega_i$  will be denoted by  $e_j, j = 1, 2, \dots, 9$ , and the internal and external energies at these points will be denoted by  $E_{in,i}^j$  and  $E_{ex,i}^j$  respectively. Thus

$$\begin{aligned}E_{in,i}^j &= a_1 V'(e_j) + a_2 V''(e_j) \\ E_{ex,i}^j &= -|I_x(e_j)| / \max_I(I_x),\end{aligned}$$

where  $V'(e_j)$  and  $V''(e_j)$  are the derivatives along the curve obtained by replacing  $v_i$  by  $e_j$ .

To allow comparison between the different energy terms, it is necessary to rescale them to the range  $[0, 1]$ .

$$\begin{aligned}\hat{E}_{in,i}^j &= \frac{E_{in,i}^j - E_{in,i}^{\min}}{E_{in,i}^{\max} - E_{in,i}^{\min}}, \\ \hat{E}_{ex,i}^j &= \frac{E_{ex,i}^j - E_{ex,i}^{\min}}{E_{ex,i}^{\max} - E_{ex,i}^{\min}},\end{aligned}$$

where the superscripts min and max denote the minimum and maximum of the respective quantities over the domain  $\Omega_i$ . Thus the contour is driven to minimise

$$\hat{E}_i = \alpha \hat{E}_{in,i} + \beta \hat{E}_{ex,i}.$$

The energy of the contour is minimised iteratively. Each iteration consists of minimising  $\hat{E}_i$  for  $i = 1, \dots, N$  consecutively. At a given step, the point  $v_i$  will be replaced to the point  $e_j$ , if

$$\hat{E}_i^j = \min \hat{E}_i^k, k = 1, 2, \dots, 9.$$

In this study the number of iteration was fixed at 30 although experiments showed that a stable contour was generally reached in only a few iterations.

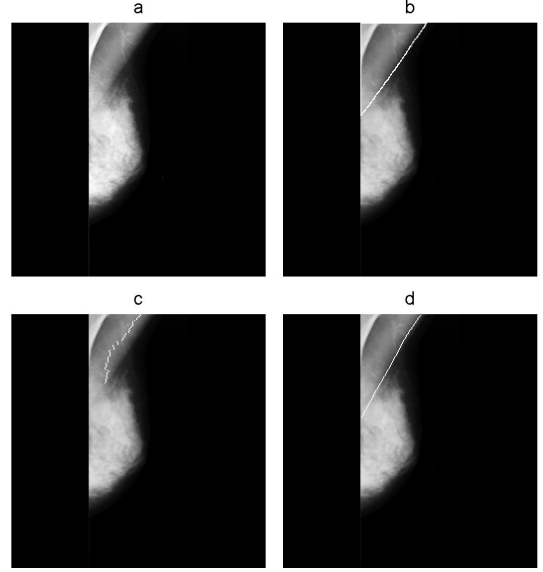


**Figure 3. Results obtained for the image mdb040. (a) Original image (b) Hand-drawn pectoral muscle edge (c) and (d) Pectoral muscle edge detected by AP method and adaptive deformable contour model, respectively.**

## 4 Experiment and Results

### 4.1 Database

83 medio-lateral oblique (MLO) mammograms, were chosen from the Mammographic Image Analysis Society (Mini-MIAS) collection. The same images were used as in the study by Ferrari, et al. [5]. All images are MLO views with  $200\text{-}\mu\text{m}$  sampling interval and 8-bit gray-level quantisation and  $1024 \times 1024$  pixels in size. To reduce the processing time, the images were down sampled to the size of  $256 \times 256$  pixels.

### 4.2 Evaluation Protocol

The same protocol for evaluation as the one used in [5] is employed in this paper to evaluate the results and to make a comparison with other methods. The extraction results of pectoral muscle boundaries of 83 images were compared with the boundaries manually identified by two radiologists

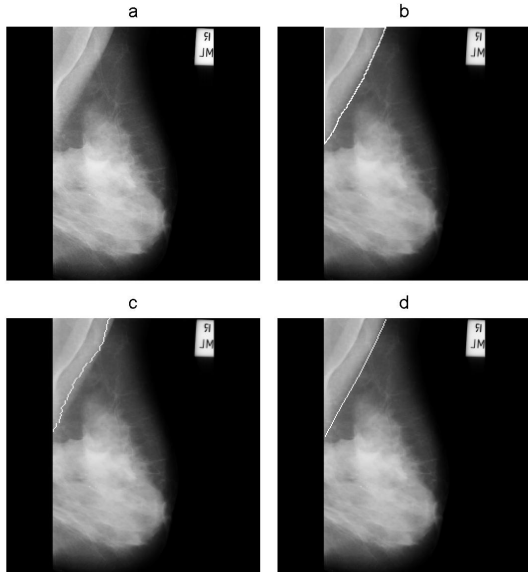


**Figure 4. Results obtained for the image mdb110. (a) Original image (b) Hand-drawn pectoral muscle edge (c) and (d) Pectoral muscle edge detected by AP method and adaptive deformable contour model, respectively.**

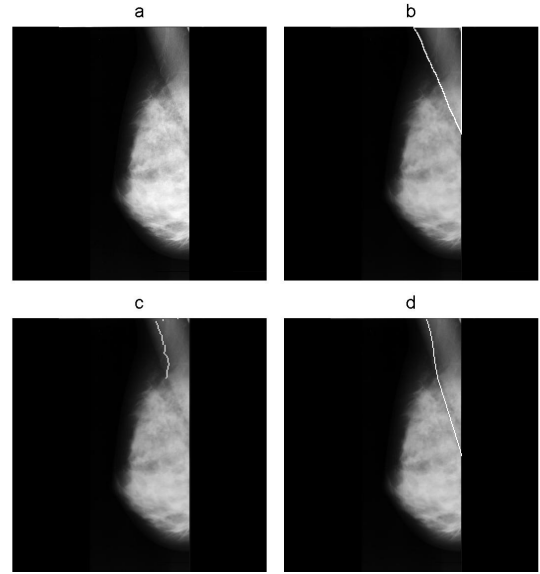


**Figure 5. Results obtained for the image mdb033. (a) Original image (b) Hand-drawn pectoral muscle edge (c) and (d) Pectoral muscle edge detected by AP method and adaptive deformable contour model, respectively.**

as reported in [5]. The pixel coordinates for the radiologists drawn boundaries were kindly supplied by R. M. Rangayyan. Since the manually identified boundaries were obtained from the original full-size images ( $1024 \times 1024$  pixels), while the results of this paper were extracted from the down-sampled images of size  $256 \times 256$ , the detection results were transferred back to the original size by interpolation. The evaluation was performed by measuring the percentages of false-positive (FP) and false-negative pixels (FN). The false-positive pixels are the pixels outside the manually drawn pectoral muscle boundary but inside the boundary marked by our results; similarly, the false-negative pixels are the pixels bounded by the manually drawn boundaries but outside our extraction results. The percentages of false-positive pixels and false-negative pixels are calculated by normalising the number of FP and FN pixels by the total amount of pectoral muscle pixels. The total number of pectoral muscle pixels was obtained by counting the pixels between the manually drawn boundary and the edge of the image.

### 4.3 Results

The mean percentages of FP and FN pixels of 83 images are 3.23% and 5.73%, respectively. For 50 images, both

FP and FN percentages were less than 5%. There are 18 images with both FP and FN percentages between 5% and 10%; and the FP or FN percentages are greater than 10% for 15 images. All the results are presented in Table 1. Table 1 also includes the results obtained by Hough and Gabor methods [5] on the same 83 mammograms.

Three examples (mdb110, mdb040 and mdb033) are shown in Figure 3, Figure 4 and Figure 5. The pectoral muscles in mdb110 and mdb040 are complex because there are many lines in the region that can be confused with the true pectoral muscle boundary. In both cases, our method works well. The pectoral muscle in mdb033 is complex and the appearance is somewhat unusual. The method did not perform particularly well on this example with percentages of FP and FN at 16% and 13%, respectively.

The processing time to perform the whole process is about 5 seconds, using a 2.8 GHz computer with 1 GB of RAM memory.

## 5 Conclusion

The proposed method (AP) performs about equally well as the method based on Gabor wavelets, both of which perform significantly better than the Hough transform method.

Methods	FP(%)	FN(%)	< 5%	5% – 10%	> 10%
Hough	1.98	25.19	10	8	65
Gabor	0.58	5.77	45	22	16
AP	3.23	5.73	50	18	15

**Table 1. Comparison of pectoral muscle detection results with Hough and Gabor [5]. The values of FP(%) and FN(%) are the average percentages of FN and FP pixels of 83 images. < 5% means the number of images with both the percentages of FN and FP smaller than 5%, 5% – 10% is the number of images with both the percentages of FP and FN between 5% and 10%, > 10% means the number of images with the percentages of FP or FN bigger than 10%**

The Hough transform models the pectoral muscle boundary as a single straight line. Both the Gabor wavelet method and the AP method allow for local deviations from a straight line and so have the flexibility to conform to more complex boundaries. In terms of the percentages of FN pixels and number of images with both the percentages of FP and FN < 5%, the method performed better than by Hough transform and Gabor methods (Table 1). The combination of AP and deformable contour described here is suitable for use in CAD systems for mammography.

## References

- [1] J. Jolion and A. Montanvert. The adaptive pyramid: A framework for 2d image analysis. *Computer Vision, Graphics, and Image Processing*, 55(3):339–348, May 1992.
- [2] N. Karssemeijer. Automated classification of parenchymal patterns in mammograms. *Phys. Med. Biol.*, 43(2):365–378, 2004.
- [3] A. Montanvert, P. Meer, and A. Rosenfeld. Hierarchical image analysis using irregular tessellations. *IEEE Transactions on Pattern Analysis and Machine Intelligence*, 13(4):307–316, April 1991.
- [4] R.J.Ferrari, R.M.Rangayyan, J.E.L.Desautels, and A.F.Frère. Segmentation of mammograms: Identification of the skin-air boundary, pectoral muscle, and fibroglandular disc. *Proc. 5th Int. Workshop Digital Mammography. M.J. Yaffe. Ed.. Toronto. ON. Canada, June 2000*, pages 573–579, 2001.
- [5] R.J.Ferrari, R.M.Rangayyan, J.E.L.Desautels, R.A.Borges, and A.F.Frère. Automatic identification of the pectoral muscle in mammograms. *IEEE Transactions on Medical Imaging*, 23(2):232–245, Feb. 2004.
- [6] S.Tanimoto and T. Pavlidis. A hierarchical data structure for picture processing. *Comput. Graphics Image Process*, 4(2):104–119, 1975.